The 6th ASME-JSME Thermal Engineering Joint Conference
March 16-20, 2003

TED-AJ03-537

THE DESIGN AND PERFORMANCE OF A WATER COOLING SYSTEM FOR A PROTOTYPE COUPLED CAVITY LINEAR PARTICLE ACCELERATOR FOR THE SPALLATION NEUTRON SOURCE

John D. Bernardin **Curtt Ammerman** **Steve Hopkins**
Mechanical Systems Group
Spallation Neutron Source Div.
Los Alamos National Laboratory
P.O. Box 1663, MS H824
Los Alamos, NM USA 87545

ABSTRACT

The Spallation Neutron Source (SNS) is a facility being designed for scientific and industrial research and development. The SNS will generate and employ neutrons as a research tool in a variety of disciplines including biology, material science, superconductivity, chemistry, etc. The neutrons will be produced by bombarding a heavy metal target with a high-energy beam of protons, generated and accelerated with a linear particle accelerator, or linac. The low energy end of the linac consists of, in part, a multi-cell copper structure termed a coupled cavity linac (CCL). The CCL is responsible for accelerating the protons from an energy of 87 MeV, to 185 MeV.

Acceleration of the charged protons is achieved by the use of large electrical field gradients established within specially designed contoured cavities of the CCL. While a large amount of the electrical energy is used to accelerate the protons, approximately 60-80% of this electrical energy is dissipated in the CCL's copper structure. To maintain an acceptable operating temperature, as well as minimize thermal stresses and maintain desired contours of the accelerator cavities, the electrical waste heat must be removed from the CCL structure. This is done using specially designed water cooling passages within the linac's copper structure. Cooling water is supplied to these cooling passages by a complex water cooling and temperature control system.

This paper discusses the design, analysis, and testing of a water cooling system for a prototype CCL. First, the design concept and method of water temperature control is discussed. Second, the layout of the prototype water cooling system, including the selection of plumbing components, instrumentation, as well as controller hardware and software is presented. Next, the development of a numerical network model used to size the pump, heat exchanger, and plumbing equipment, is discussed. Finally, empirical pressure, flow rate, and temperature data from the prototype CCL water cooling tests are used to assess water cooling system performance and numerical modeling accuracy.

NOMENCLATURE

Symbol	Description
K	Flow loss coefficient
Q	Volumetric flow rate
q	Heat transfer rate
T	Temperature
UA	Overall heat transfer coefficient
v	Velocity
DP	Pressure drop
r	Density

INTRODUCTION

The Spallation Neutron Source (SNS) is a facility being designed in a collaborative effort between six national laboratories for scientific and industrial research and development (see Fig. 1). The SNS will generate and employ neutrons as a research tool in a variety of disciplines including biology, material science, superconductivity, chemistry, etc. The neutrons will be produced by bombarding a heavy metal target with a high-energy beam of protons, generated and accelerated with a linear particle accelerator, or linac.

The low energy end of the linac consists of, in part, a multi-cell copper structure termed a coupled cavity linac (CCL). The CCL, partially shown in Fig. 1, is responsible for accelerating the protons from an energy of 87 MeV, to 185 MeV. The CCL is comprised of four modules. Each module is made up of twelve segments, with each segment housing eight accelerator cavities and side coupling cells (SCCs), the latter of which serve to electrically join neighboring cavities. Between each segment is a copper bridge coupler cavity, which provides electrical continuity

between the adjoining segments. Additional design details on accelerator structures can be found in [1, 2].

RF electrical energy is fed into the accelerator cavities and bridge couplers to provide high gradient electrical fields that serve to accelerate the protons. While a large amount of the electrical energy is used to accelerate the protons, approximately 60-80% of this electrical energy is dissipated in the CCL's copper structure. To maintain an acceptable operating temperature, as well as minimize thermal stresses and maintain desired contours of the accelerator cavities, the electrical waste heat must be removed from the CCL structure. This is done using forced convection cooling with specially designed water cooling passages within the linac's copper structure. The internal cavity and SCC water cooling passages are displayed in an exploded view of Fig. 1. The bridge coupler cooling passages consist of copper coils that are brazed to the outer cylindrical surface, as displayed in Fig. 1. More details on these cooling passages as well as the finite element and computational fluid dynamics numerical models employed to optimize their designs and the water flow rates, can be found in [3]. Table 1 summarizes the heat loads and required water cooling flow rates and temperatures for the various CCL components.

Table 1. Summary of the heat loads and required water cooling flow rates and temperatures for the prototype CCL.

Component	Heat Load [W]	Water Flow Rate [Lpm] (gpm)	Water Inlet Temp. and Range [°C]
Individual Cavity	1,073	9.5 (2.5)	25.0 ±7.5
Individual SCC	119	0.95 (0.25)	25.0 ±7.5
Bridge Coupler	500	3.8 (1.0)	25.0 ±7.5
Segment of 8 Cavities and SCCs	9,545	83.6 (22.0)	25.0 ±7.5
Entire CCL Prototype	19,590	171 (45.0)	25.0 ±7.5

Cooling water is supplied to the CCL cooling passages by a closed-loop water cooling and temperature control system, similar to those used on other linacs [4, 5]. A highly simplified flow diagram of such a closed-loop temperature control system is shown in Fig. 2(a). In this loop, water is pumped at a constant flow rate to the linac, where it picks up heat. On the return leg, a 3-way valve directs a portion of the flow through a liquid-to-liquid heat exchanger to dump heat to a chilled water source, while the remainder of the water is diverted through a by-pass line. These two flows then recombine before entering the pump for circulation back to the linac. In this closed-loop circuit, water temperature control is achieved by manipulating the hot side (linac side) heat exchanger water flow rate while holding the cold-side water inlet temperature and flow rate constant. By changing the hot-side water flow rate, the overall heat transfer coefficient of the heat exchanger is varied. Since the heat removal rate must effectively remain constant for a quasi-steady-state condition, the heat exchanger's hot-side water temperature must change inversely to the overall heat transfer coefficient to achieve a new and balanced operating condition. Consequently, increasing the water flow through the heat exchanger results in an increase in the overall heat transfer coefficient, and an associated decrease in the mean outlet water temperature. And conversely, decreasing the water flow through the heat exchanger results in a decrease in the overall heat transfer coefficient, and an associated increase in the mean outlet water temperature. The outlet water temperature dependence on the heat exchanger hot-side flow rate is depicted in Fig. 2(b). Figure 2(a) is a simplified view of the actual water cooling system design. More detailed descriptions of the cooling system are provided in the next section.

This paper discusses the design, analysis, and testing of a water cooling system for a prototype CCL. First, the design layout of the prototype water cooling system, including the selection of plumbing components, instrumentation, as well as controller hardware and software is presented. Next, the development of a numerical network model used to size the pump, heat exchanger, and plumbing equipment, is discussed. Finally, empirical pressure, flow rate, and temperature data from the prototype CCL water cooling tests are used to assess water cooling system performance and numerical modeling accuracy.

WATER COOLING SYSTEM DESIGN AND EXPERIMENTAL APPARATUS

Figure 3 displays a prototype CCL that was built to test the design and manufacturing concepts of the linac, as well as the performance of the water cooling and temperature control system. As the schematic of Fig. 3 indicates, the CCL prototype is comprised of two 8-cavity OFC copper segments joined by an OFC copper bridge coupler and mounted on a support stand. Figure 3 also displays several subsystem interfaces for the CCL including the vacuum pumping equipment, the RF window, which is the interface connection between the RF waveguide and the CCL, and a large number of water cooling lines.

Figure 4(a) displays the piping and instrumentation diagram of the prototype CCL water cooling system. The heart of the water cooling system is the water skid, or the components that lie within the dashed outline of Fig. 4(a). The water skid is a self-contained unit with all of the necessary plumbing, water purification hardware, instrumentation, pumping, and heat transfer equipment required for delivering water at a desired flow rate, purity, and temperature to the CCL RF structure. The prototype water skid fabricated for this study is displayed in Fig. 5.

A small capacity tank served as a water reservoir and allowed for expansion and contraction of the water associated with temperature changes. The tank was equipped with a Nitrogen gas source for controlling system pressure and reducing the presence of dissolved oxygen in the water. A pressure relief valve, vent valve, and a liquid low-level indicator were added to the tank for

safety purposes. The water reservoir fed the main water line on the suction side of the pump through a manual valve. The reservoir tank capacity was kept below 38 Liters (10 gal) to minimize the effect of its thermal mass on the time response of the water loop's temperature control system.

A high capacity, variable speed centrifugal pump (R.S. Corcoran Co., Series 4000, Model DVL-FAB (AA)), rated at 380 Lpm @ 455 kPa (100 gpm @ 65 psig), with a maximum dead head pressure of 630 kPa (90 psig), was selected to supply a constant water flow rate to the RF structure.

To provide for heating of the water loop, a 34 kW inline electrical water heater was placed downstream of the pump. A manual ball valve, plumbed in parallel with the heater, was used to direct all of the water flow through the heater when it was in use. To remove the waste heat from the cooling loop and maintain the desired water temperature, a stainless steel flat plate counter-flowing heat exchanger (Flat Plate Inc., FP10*20-60) was incorporated. The cold side of the heat exchanger was supplied with refrigerated water from a water chiller (Cooling Technology, Inc., Model CPCW-35) possessing a maximum flow capacity of 570 Lpm @ 307 kPa (150 gpm @ 44 psig), and a rated heat removal capacity of 115 kW @ 10°C delivery temperature. The chiller's waste heat was dumped to a facility-supplied, evaporative cooling water circuit.

The water temperature in the flow loop was manipulated by adjusting the distribution of water flow between the heat exchanger and the heat exchanger by-pass line (see Fig. 4). This was achieved using a proportional 3-way valve (A-T Controls Inc., Series 30, Model 30-F1-150/TED2-XX-T) upstream of the heat exchanger. The 3-way valve split the water flow between the heat exchanger and a by-pass line.

A water purification system was included in the design of the water skid to minimize the formation of deposits, scale buildup, biological growth, corrosion and radionuclide activation. This system consisted of $5*10^{-6}$ m and a $1*10^{-6}$ m filter for removal of debris, a carbon bed for extraction of hydrocarbons, several ion exchange resins for the removal of salts and minerals, an oxygen scavenger to remove dissolved oxygen, and an ultraviolet lamp to kill bacteria. The water treatment hardware was placed in a small side loop through which approximately 3% of the total flow was circulated. Electrical resistivity, pH, and dissolved oxygen sensors were used to monitor the water purification system performance. A sampling port was provided to monitor particulates, total organic carbon, bacteria counts, and trace elements. More specific details concerning the criteria, design, and performance of the water purification system can be found in [3, 6].

The water skid delivered cooling water to a main supply manifold, which distributed the water to the CCL cavities, side coupling cells, and bridge coupler by way of multiple distribution lines, as shown in the piping and instrumentation diagram of Fig. 4(b). A corresponding set of water lines served to transfer the cooling water back to the water skid upon exiting the CCL. Globe valves on the supply lines and flow meters on the return lines, were used to accurately meter the correct amount of water to each set of CCL components.

The majority of the plumbing was fabricated from copper pipe and fittings, as well as flexible buna-n hoses, while the valves, strainers, and other components were comprised of 316 stainless steel.

A variety of transducers, shown in Fig. 4, were strategically placed on the water skid and on the CCL supply and return lines to record water temperature, pressure, and flow rate. Platinum wire wound RTDs (100 Ohm, 3 lead, European calibration) with a calibrated accuracy of ±0.1°C, were used to measure water temperatures. System pressures were measured with transducers with a 0-699 kPag (0-100 psig) full scale range and an accuracy of 2.8 kPa (0.4 psi). Paddle wheel flow meters, with an accuracy of ±6.1 cm/s (± 0.2 ft/sec) were used to monitor flow rates in water lines with internal diameters of 2.54 cm (1 in.) and larger. Turbine flow meters, with an accuracy of 1%, were used on water lines with an internal diameter of 0.95 cm (0.375 in.). To minimize electrical noise and interference, all instrumentation and communication cables were shielded and electrically grounded. Several of the transducers were used for flow and temperature control purposes during operation, while the remainder were employed for system monitoring as well as energy balance and pressure drop calculations.

All transducers, as well as the 3-way control valve, were connected to a FieldPoint distributed input/output and data acquisition system, which was supervised with a PC running Labview 5.0 software. The Labview 5.0 software acquired all of the water purity, temperature, pressure, and flow rate data at a periodic rate defined by the operator. Water temperature control was achieved with a Labview PID algorithm to manipulate the position of the 3-way valve. The PID algorithm employed a user-supplied water temperature set-point and a user-defined RTD temperature reading as the feed-back variable. Specific details on the design and operation of the temperature control system software can be found in [7].

Before the prototype CCL water cooling system tests could be conducted, the correct flow distribution had to be established. This was achieved by circulating water through the entire system and manually adjusting the globe valves on the CCL water inlet lines, the water purification loop, and the pump by-pass loop. Flow rates were continuously monitored throughout the system to obtain the necessary valve settings. Next, the water chiller was turned on and the water supply temperature and flow rate were set. Next, the two electrical water heaters were turned on to supply a steady-state heat load to the system. Finally, the water temperature control system was activated and the desired CCL water inlet temperature set-point was programmed into the control system software. At this point, the Labview PID algorithm maintained the

desired water temperature through control of the 3-way valve position, and the data acquisition system continuously logged the system's water temperatures, pressures, and flow rates.

Once the water cooling system was functioning properly, the performance testing of the CCL prototype and its water cooling and temperature control system was initiated. During these tests, RF power at various amplitudes, frequencies, and pulse lengths, was applied intermittently to the prototype CCL. The total average RF power was gradually increased to the design level of 19.59 kW for the prototype CCL. Throughout the tests, the temperature, pressure, and flow rate data from the water cooling system, as well as the RF parameters, were periodically recorded.

NUMERICAL MODELS

To support the design and optimization of the water cooling system, a representative numerical model of the prototype CCL water cooling system was developed using the software package SINDA/FLUINT [8]. This model aided in the sizing of the water cooling system components so that the cooling parameters listed in Table 1 could be met.

SINDA/FLUINT uses a nodal network modeling approach to represent a complex flow system as a series of lumps, where pressure and temperature are calculated, connected by path lines, where flow resistance is defined and flow rate is calculated. Figure 6 illustrates the SINDA/FLUINT representation of a basic flow loop. Lumps may be described by a tank, T-10, where energy and mass can change with time, or they may be represented by a simple junction, J, which is a tank of zero volume. Path lines can be made up of one of many different elements including tubes, T, of a given length and diameter, a valve, CT, with a variable flow resistance, a pressure loss, L, to account for a fitting or pipe bend, a constant volume pump, VF, etc. A SINDA/FLUINT model may also employ a "Tie" element that is used to join fluid submodels with thermal submodels, such as those required in a heat exchanger calculation. More specific SINDA/FLUINT modeling capabilities can be found in [8].

Two separate SINDA/FLUINT models were built for this study. The first, termed the CCL segment and Bridge Coupler model, was used to represent the water lines and cooling passages between the supply and return manifolds on the CCL. This highly detailed model was used to determine the pressure drops across the CCL cooling passages and water supply and return lines. The second model, termed the Water Skid and Flow Loop Model, characterized the entire CCL flow loop, with an emphasis on the water skid components including the pump, heater, and control valve. This model was used to determine the entire system pressure drop and calculate the CCL water supply temperature as a function of the heat exchanger hot side flow rate. More specific features of these two models are discussed below.

CCL Segment and Bridge Coupler Model

The SINDA/FLUINT model of the 8-cavity CCL segment and bridge coupler is shown in Fig. 7 alongside an equivalent 3-D representation and flow diagram. The model consists of three main cooling circuits, one for the bridge coupler (BC), one for the side coupling cells (SCCs), and one for the accelerator cavities. Each cooling circuit within the model is made up of a number of tube, loss, and valve elements to account for the lines, fittings, bends, cooling passages and valves shown in Fig 7(a).

The SINDA/FLUINT input for a tube includes a length and a diameter dimension, and the output consists of the pressure drop corresponding to a defined flow rate. The modeling input for a valve, CT, and a loss, L, consists of the flow passage cross sectional area and a dimensionless "*K*" or loss coefficient, defined as [9]

$$K = 2\,DP / (r\,v^2), \qquad (1)$$

where, *DP* is the pressure loss across the segment, *r* is the fluid density, and *v* is the mean fluid velocity.

The numerical values for the various tube, loss, and valve elements shown in Fig. 7(b), are summarized in Table 2. Note that the loss factors for the valves were left as floating variables that were adjusted in the numerical model to obtain the desired flow rates in the cavities, SCCs, and BC. The valve loss factors that provided the desired flow distribution, are listed in Table 2. The majority of the loss factors listed in Table 2 are summations of multiple loss factors corresponding to the many fittings and bends that make up the CCL water lines. More detailed information concerning the precise geometry and make-up of the CCL's internal cooling passages and water lines, as well as the associated loss coefficients, can be found in [3].

Water Skid and Flow Loop Model

The SINDA/FLUINT model of a simplified water skid and flow loop is shown in Fig. 8 alongside an equivalent flow diagram. To reduce the complexity of the modeling process, the water purification and pump by-pass loops were left out of the water skid model since they would not significantly influence the overall system pressure drop or temperature control predictions.

The numerical model consists of a number of tube, loss, and valve elements to account for the lines, fittings, bends, and valves. An equivalent loss element, L2, was used to represent the water lines and cooling passages of the CCL RF structure. The equivalent loss factor for L2 was determined from the CCL segment model shown previously in Fig. 7. Using a pressure drop of 65.7 kPa (9.4 psi), a flow rate of 171 Lpm (45 gpm) through the CCL RF structure, and a hydraulic diameter of 5.08 cm (2.0 in.) for the simulated RF structure loss element, resulted in a loss factor of 64.7. All of the tube and loss

Table 2. Tube, loss, and valve parameters for the CCL 8-cavity segment model.

Symbol & Description	Tube or hydraulic dia. [cm]	Length [cm]	K factor
T1: Outer cooling circuit line	7.6	30.5	0.0
T2: BC supply line	1.0	58.4	0.0
T3: BC body cooling lines	0.3	88.9	12.5
T4: BC slug tuner cooling lines	1.0	88.9	4.8
T5: BC return line	1.0	101.6	0.0
T6: SCC main supply line	1.0	27.9	0.0
T7: SCC top grouping supply line	1.0	55.9	0.0
T8: SCC bottom grouping supply line	1.0	27.9	0.0
T9: SCC supply & return sub-manifold run lengths between SCC ports	1.0	10.2	0.0
T10: Individual SCC supply line	1.0	25.4	0.0
T11: SCC cooling passage	0.3	53.3	0.0
T12: Individual SCC return line	1.0	10.2	0.0
T13: SCC top grouping return line	1.0	12.7	0.0
T14: SCC bottom grouping return line	1.0	40.6	0.0
T15: SCC main return line	1.0	175.3	0.0
T16: Cavity main supply line	2.5	66.0	0.0
T17: Cavity top grouping supply line	2.5	7.6	0.0
T18: Cavity bottom group supply line	2.5	165.1	0.0
T19: Cavity internal headers	2.5	6.4	0.0
T20: Cavity top grouping return line	2.5	154.9	0.0
T21: Cavity bottom group return line	2.5	15.2	0.0
T22: Cavity main return line	2.5	55.9	0.0
L1: BC supply line losses	1.0	N/A	3.6
L2: BC body cooling channel lossses	0.3	N/A	4.1
L3: BC slug tuner channel losses	1.0	N/A	8.9
L4: BC return line losses	1.0	N/A	3.57
L5: SCC main supply line losses	1.0	N/A	3.64
L6: SCC top group supply line losses	1.0	N/A	2.06
L7: SCC bottom group supply line loss	1.0	N/A	1.86
L8: Individual SCC supply line losses	1.0	N/A	3.69
L9: SCC cooling passage losses	0.3	N/A	1.00
L10: Individual SCC return line losses	1.0	N/A	3.69
L11: SCC top group return line losses	1.0	N/A	1.82
L12: SCC bottom group return line loss	1.0	N/A	2.06
L13: SCC main return line losses	1.0	N/A	4.00
L14: Cavity main supply line losses	2.5	N/A	3.76
L15: Cavity top group supply line loss	2.5	N/A	0.86
L16: Cavity bottom group supply loss	2.5	N/A	2.40
L17: Cavity cooling passage losses	1.3	N/A	75.0
L18: Cavity top group return line losses	2.5	N/A	3.00
L19: Cavity bottom group return loss	2.5	N/A	0.86
L20: Cavity main return line losses	2.5	N/A	5.86
CT1: BC valve	1.0	N/A	142.2
CT2: SCC valve	1.0	N/A	24.4
CT3: Cavity valve	2.5	N/A	0.7

factor values for the water skid and flow loop model are summarized in Table 3. A more detailed breakdown of the water skid component's loss coefficients is given in [3].

A heat-input element, used to represent the heat dissipation from the RF structures and water heater, was placed immediately downstream of the RF structure loss element. A constant flow rate pump element, VF, was used to represent the performance of a centrifugal pump. SINDA/FLUINT was not capable of modeling a 3-way control valve. Therefore, a 2-way proportional valve was modeled in the heat exchanger by-pass line. This valve configuration closely emulated the flow conditions encountered with the 3-way valve over the majority of its operational range. However, the use of the 2-way valve did not allow for the modeling condition where all of the water was by-passed around the heat exchanger.

Finally, a thermal sub-model of the heat exchanger was included in the water skid model. The development of this thermal sub-model first required the sizing of a commercially available flat plate heat exchanger to meet the temperature, heat load, and flow rate requirements listed in Table 1 [3], while providing reasonable pressure drops. Once the heat exchanger was selected, its thermal performance was incorporated in the numerical model in the form of a correlation that related the heat exchanger's overall heat transfer coefficient, *UA*, to the hot side water flow rate, Q_h, for a constant cold side flow rate:

$$UA = (25.3Q_h + 65.7)/(Q_h+8) \text{ for } Q_c = 72.2 \text{ Lpm}, \quad (2)$$

$$UA = (63.3Q_h + 164.3)/(Q_h+17) \text{ for } Q_c = 551 \text{ Lpm}, \quad (3)$$

where the units for *UA* are W/°C and for Q_h are Lpm.

Table 3. Tube, loss, and valve parameters for water skid model.

Symbol & Description	Tube or hydraulic dia. [cm]	Length [cm]	K factor
T1: Water skid outlet line	3.8	309.9	0.0
T2: RF structure supply transfer line	5.1	365.8	0.0
T3: RF structure return transfer line	5.1	365.8	0.0
T4: Water skid inlet line	5.1	50.8	0.0
T5: Heat exchanger inlet line	3.8	38.1	0.0
T6: Heat exchanger line	3.8	2.5	0.7
T7: Heat exchanger outlet line	3.8	144.8	0.0
T8: Heat exchanger by-pass line	3.8	22.9	0.0
T9: Pump inlet line	3.8	132.1	0.0
L1: Water skid outlet line losses	3.8	N/A	12.2
L2: Equiv. CCL RF structure loss	5.1	N/A	64.7
L3: Water skid inlet line losses	3.8	N/A	2.1
L4: Heat exchanger inlet line losses	3.8	N/A	1.5
L5: Heat exchanger outlet line losses	3.8	N/A	6.7
L6: By-pass line manual valve loss	3.8	N/A	1.8
L7: Pump inlet line losses	3.8	N/A	1.1
CT1: 2-way control valve	3.8	N/A	Vary

RESULTS

Pressure Drop Predictions versus Measurements

Table 4 provides a comparison between the numerically predicted and the experimentally measured pressure drops across the CCL RF structural components, as well as the entire RF structure and the water skid's pump. Note that while the flow rates were specified in the numerical model prior to the experiments, they had to be manually adjusted with proportional valves in the experimental set-up. Consequently, there are some minor discrepancies between the numerical and experimental flow rates. The error ranges for the empirical flow rate and pressure drop measurements, correspond to the accuracy limitations of the respective transducers. As

Table 4 indicates, the numerical model did quite well to predict the pressure drops across the cavities, SCCs, and BC. In each case, the numerically predicted pressure drop is within, or just outside, the empirical accuracy range of the corresponding measured value. The discrepancies can be attributed primarily to the flow rate differences between the model and experiment.

Table 4. Comparison of predicted and measured pressure drops within the CCL RF structure and water skid.

Component	SINDA/FLUINT Model Prediction		Experimental Measurement	
	Flow Rate [Lpm] (gpm)	Pressure Drop [kPa] (psi)	Flow Rate [Lpm] (gpm)	Pressure Drop [kPa] (psi)
Upper Cavities	30.8 (8.1)	39.2 (5.6)	33.1 ±1.9 (8.7 ±0.5)	42.7 ±2.8 (6.1 ±0.4)
Lower Cavities	38.4 (10.1)	38.5 (5.5)	39.1 ±1.9 (10.3 ±0.5)	39.9 ±2.8 (5.7 ±0.4)
Upper SCCs	3.0 (0.8)	12.6 (1.8)	3.4 ±0.04 (0.9 ±0.01)	7.7 ±2.8 (1.1 ±0.4)
Lower SCCs	3.8 (1.0)	12.6 (1.8)	3.4 ±0.04 (0.9 ±0.01)	7.7 ±2.8 (1.1 ±0.4)
BC	4.2 (1.1)	5.6 (0.8)	4.2 ±0.04 (1.1 ±0.01)	9.8 ±2.8 (1.4 ±0.4)
RF Structure	364.8 (96.0)	142.5 (20.4)	358.3 ±4.2 (94.3±1.1)	138.3 ±2.8 (19.8±0.4)
Pump	364.8 (96.0)	593.1 (84.9)	358.3 ±4.2 (94.3±1.1)	569.4 ±2.8 (81.5±0.3)

Water Temperature Predictions versus Measurements

In addition to the pressure drop assessments, an equally important task of the numerical modeling, was to predict the CCL RF structure water supply temperature, using the temperature control methodology discussed previously. Figure 9 displays numerical predictions of the CCL water inlet temperature as a function of the heat exchanger's hot side water flow rate for different heat loads, q, as well as various heat exchanger cold side flow rates, Q_c, and cold side water inlet temperatures, T_{ci}. Also plotted in Figure 9 are experimental measurements of the CCL water supply temperature for various conditions. The experimental data corresponds quite well with the numerical predictions, displaying agreement with both the absolute temperature values and the trends. More importantly, the experimental data indicates that the water cooling system provided both the necessary cooling of the RF structure and the required water temperature control.

CONCLUSIONS

This study focused on the design, analysis, and testing of a water cooling and temperature control system for a prototype coupled cavity linear particle accelerator (CCL). As part of this study, two numerical flow network models were developed for the CCL RF structure and water cooling skid, and benchmarked with empirical water flow rate, pressure, and temperature data collected from a prototype CCL water cooling system. From the numerical analysis and experimental measurements, the following key conclusions can be drawn:

1. The water cooling and temperature control system design, aided with the pump and heat exchanger sizing information from the numerical model, adequately met the heat removal and temperature regulation requirements of the CCL.
2. The numerical flow network models possessed sufficient accuracy to predict pressure drops within the CCL RF structure and water cooling skid. In addition, the numerical water skid model accurately predicted the CCL RF structure water supply temperature, using the temperature control methodology outlined in this study.
3. The accuracy of the modeling results demonstrates that flow network modeling, including the selection of flow loss coefficients and modeling of heat exchangers, can be successfully employed in designing a complex water cooling system.

REFERENCES

[1] Wangler, T., 1998, "RF Linear Accelerators," John Wiley and Sons, Inc., NY.

[2] Chao, A.W., and Tigner, M., 1999, "Handbook of Accelerator Physics and Engineering," World Scientific Publishing Company, NJ.

[3] Bernardin, J.D., Brown, R. Brown, S., Bustos, G., Crow, M., Gioia, J., Gregory, W., Hood, M., Jurney, J., Katonak, D., Konecni, Z., Marroquin, P., Medalen, I., and Weiss, R., 2001, "Spallation Neutron Source Coupled Cavity Linac Water Cooling and Resonance Control System Final Design Report," LA-UR-02-1214, Los Alamos National Laboratory.

[4] Dortwegt, R., Pasky, S., and White, M., 1999, "Improved Temperature Regulation of APS Linac RF Components," Proceedings of the 19th International Linear Accelerator Conference, Chicago, IL.

[5] Floersch, R., Domer, G., and Jett, N., 1999, "Resonance Control Cooling System for the APT/LEDA CCDTL Hot Model," Proceedings of the 18th Particle Accelerator Conference, NY, NY.

[6] Katonak, D., Bernardin, J., and Hopkins, S., 2001, "Water Purity Development for the Coupled Cavity Linac (CCL) and Drift Tube Linac (DTL) Structures of the Spallation Neutron Source (SNS) Linac," *Proceedings to the 2001 Particle Accelerator Conference*, TPAH097, Chicago, IL.

[7] Treml, C.A., Brown, S.K., and Bernardin, J.D., 2001, "Resonance Control Cooling System for a Proto-type Coupled Cavity Linac," *Proceedings to the 8th International Conference on Accelerator and Large Experimental Physics Control Systems*, WEAPO76, San Jose, CA.

[8] SINDA/FLUINT, 1988, General Purpose Thermal/Fluid Network Analyzer, Version 4.1, User's Manual, Cullimore and Ring Tech., Inc., Littleton, CO.

[9] Idelchik, I. E., 1996, "Handbook of Hydraulic Resistance," 3rd ed., Begell House, Inc., NY.

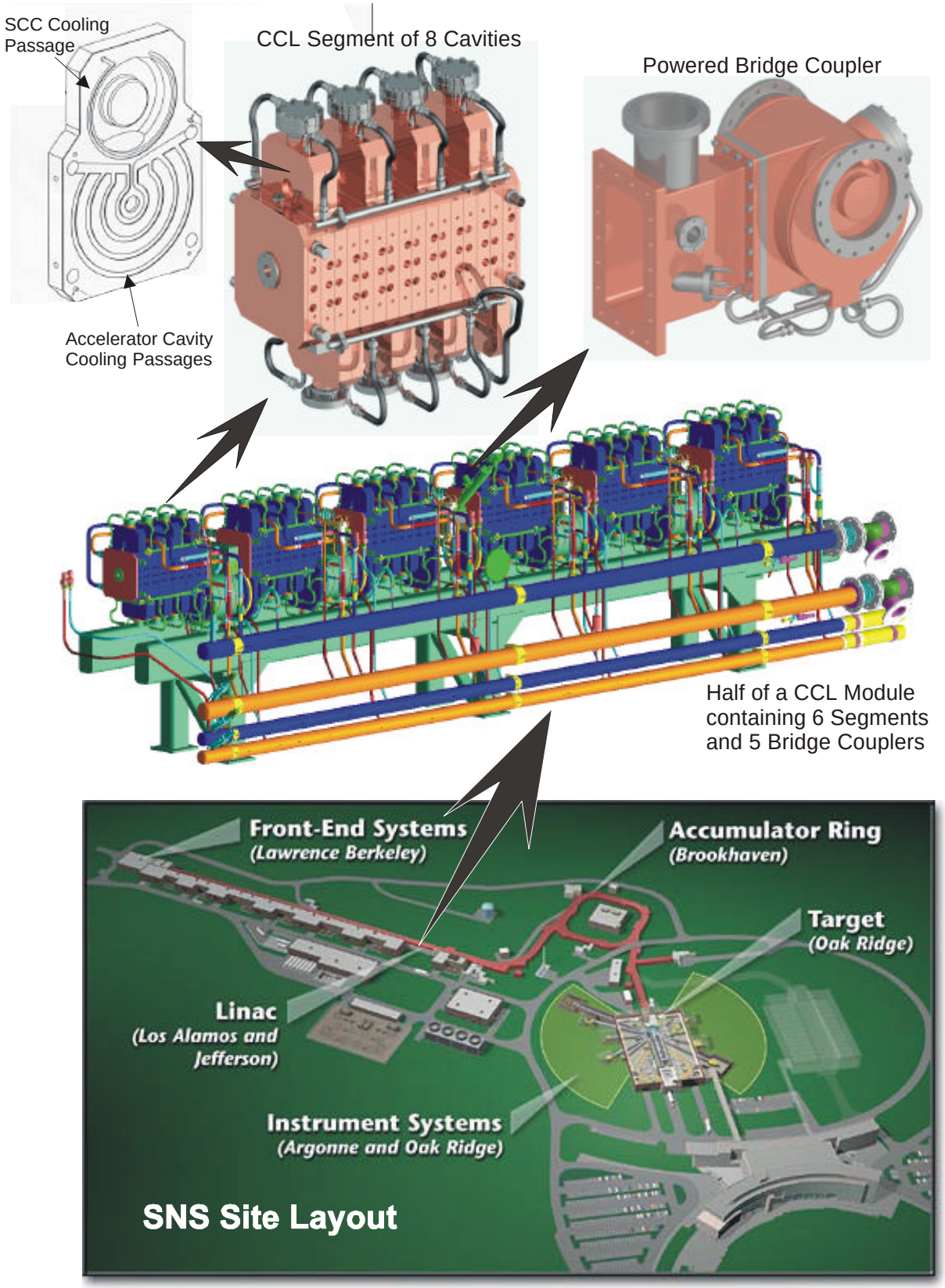

Figure 1. Schematic layout of the SNS, with exploded views of half a CCL module and its major R F structure components.

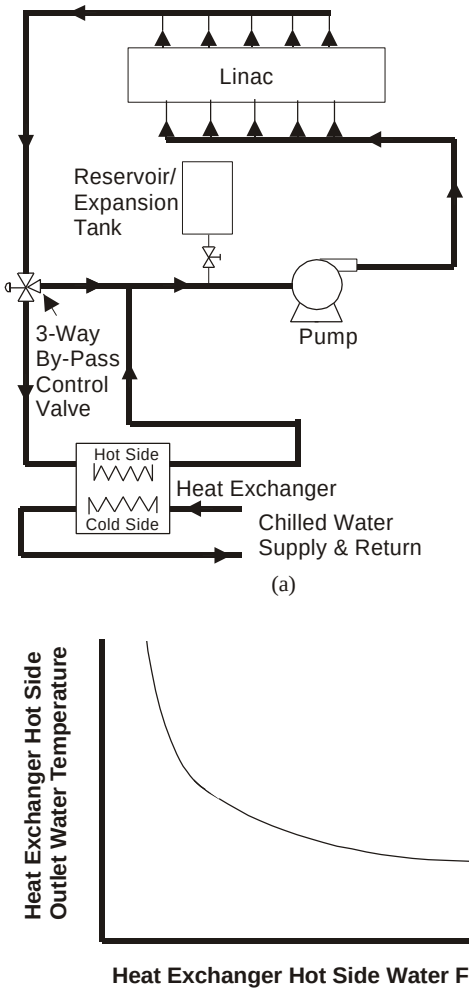

Figure 2. (a) Closed-loop linac water cooling system flow diagram and (b) water temperature vs. heat exchanger hot-side flow rate.

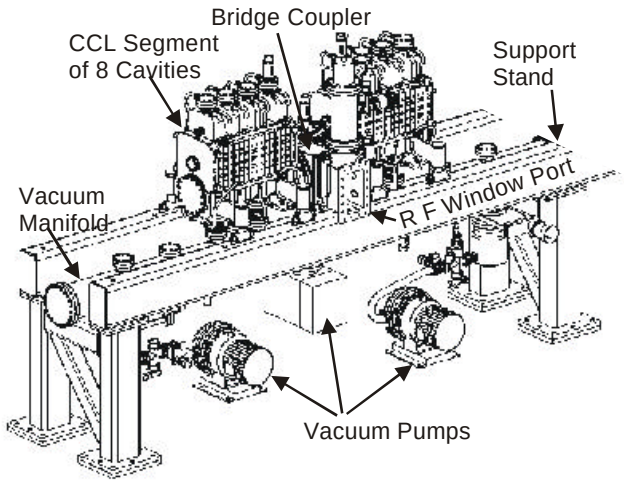

Figure 3. Schematic of the prototype CCL RF structure shown without the majority of the water cooling lines.

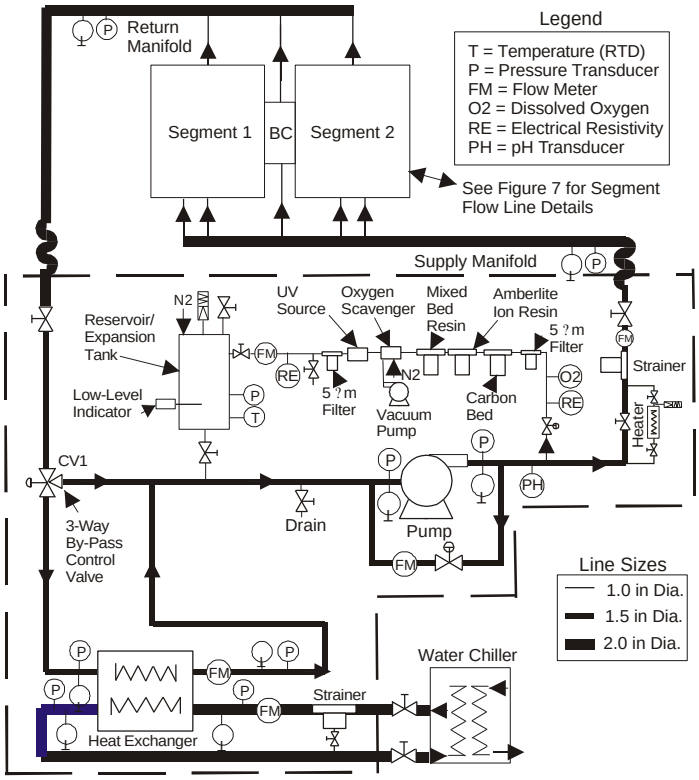

Figure 4. Piping and Instrumentation diagram of the prototype CCL water cooling system.

Figure 5. Photograph of the prototype water cooling and temperature control skid.

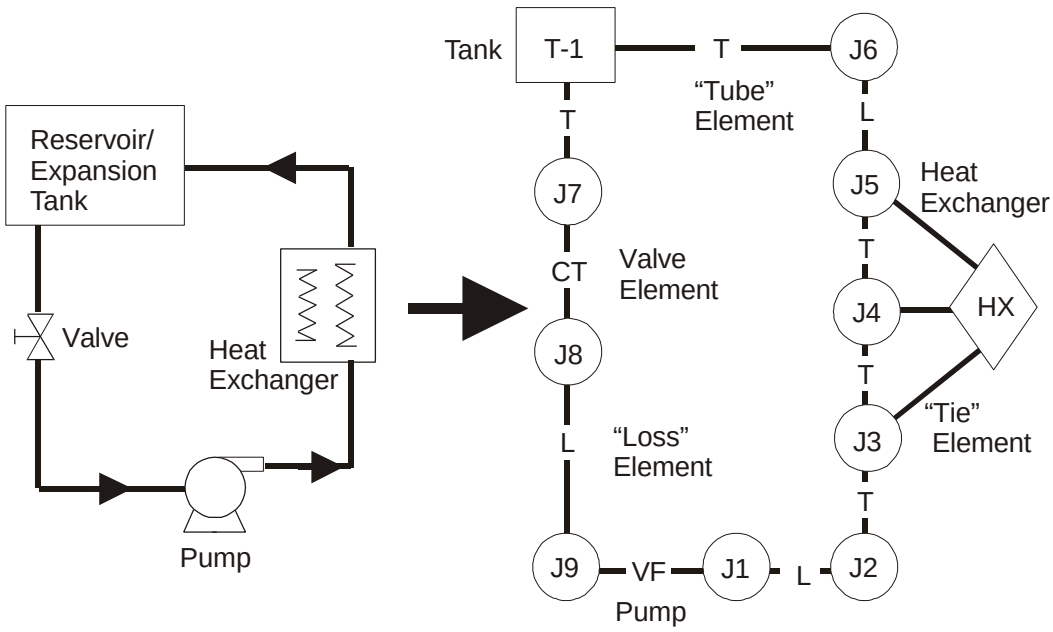

Figure 6. SINDA/FLUINT representation of a flow system.

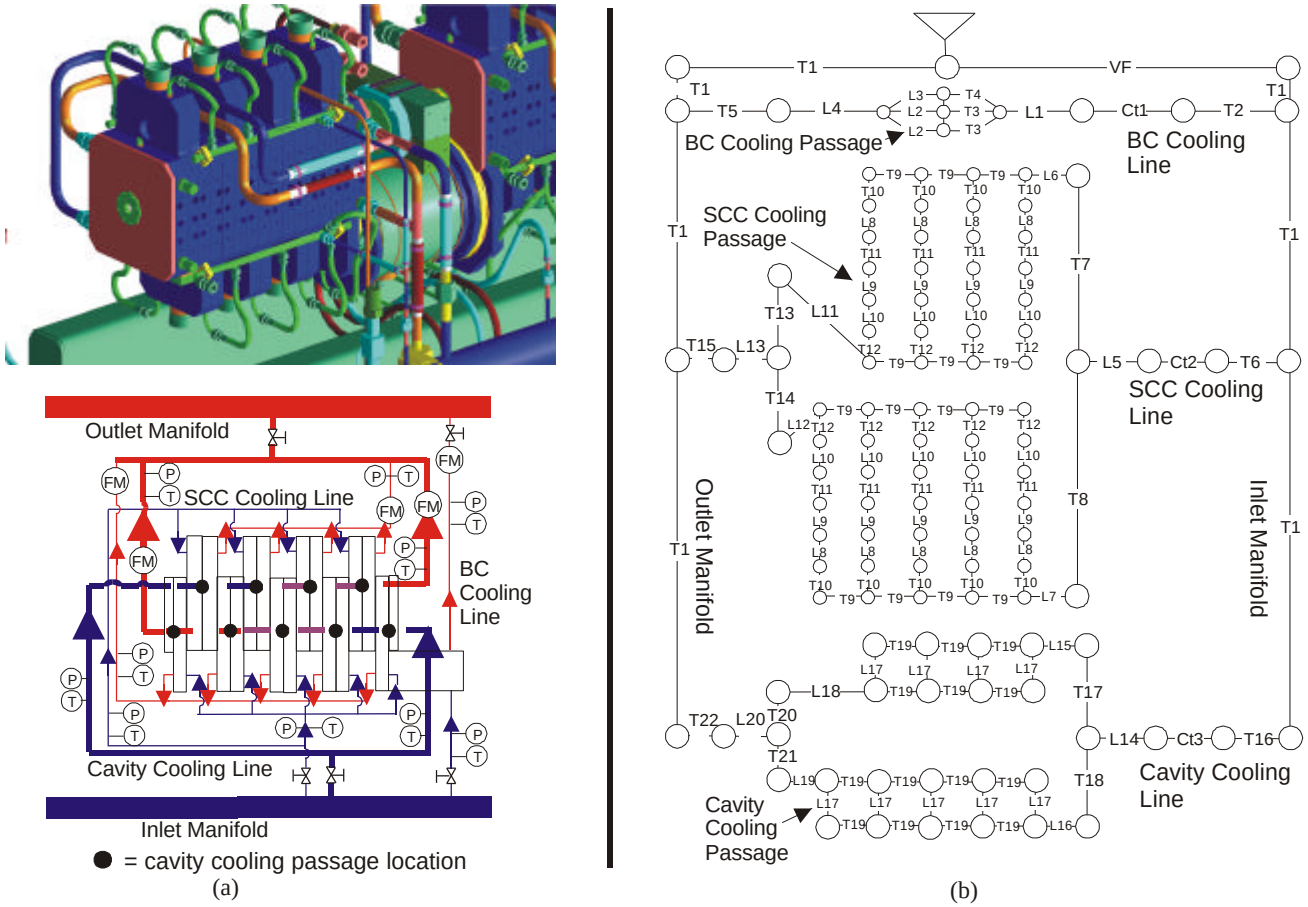

Figure 7. (a) CCL 8 cavity segment and bridge coupler model3-D representation and flow diagram and (b) corresponding Sinda/Fluint model.

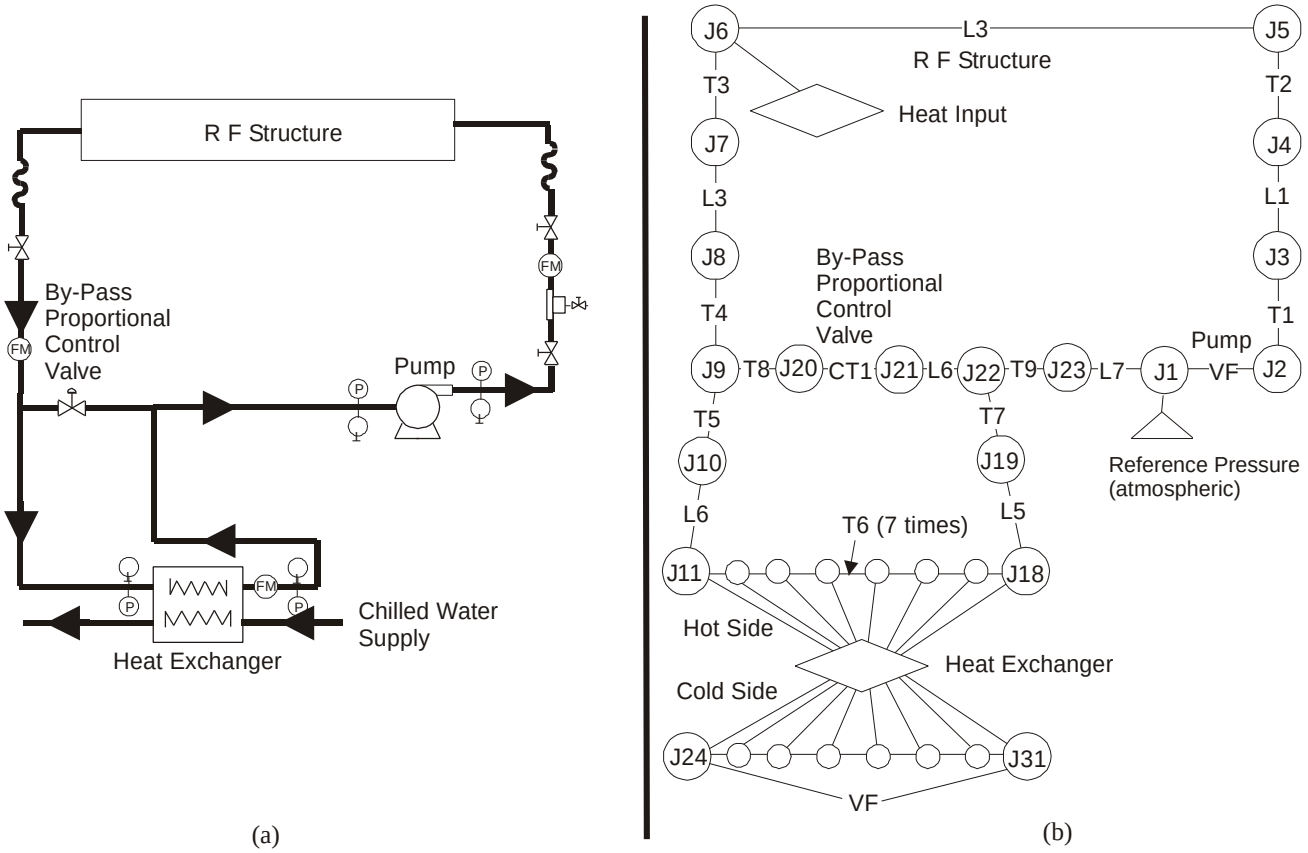

Figure 8. (a) Flow diagram of the prototype CCL water flow loop and (b) corresponding SINDA/FLUINT model.

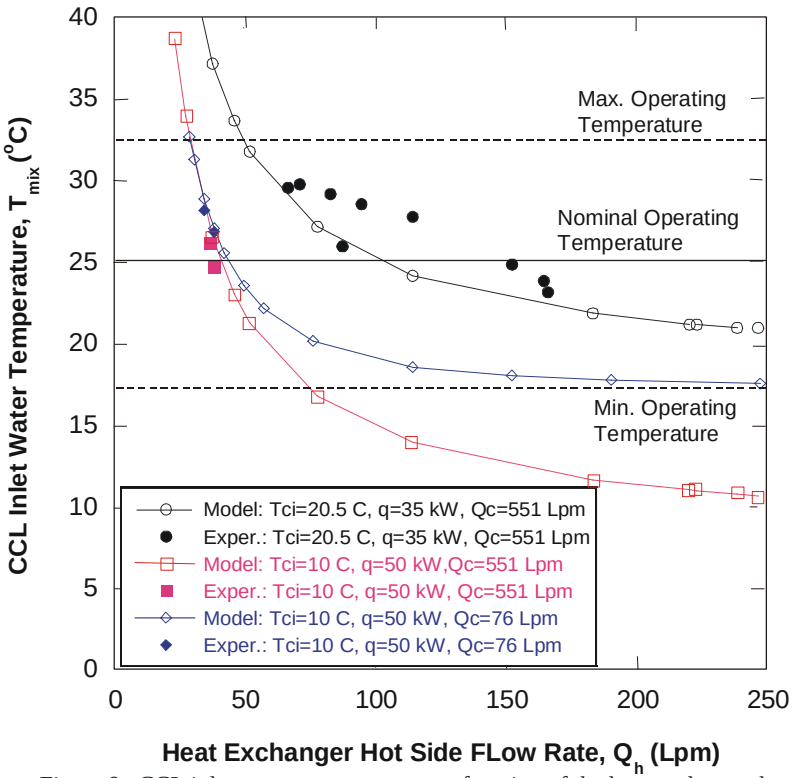

Figure 9. CCL inlet water temperature as a function of the heat exchanger hot side flow rate for various heat loads, q, as well as heat exchanger cold side water inlet temperatures, Tci, and flow rates, Qc.